journal of the American Ceramic Society

Microstructure and electrical properties of Nb-doped SrTiO3-based lead-free ceramics

Journal:	*Journal of the American Ceramic Society*
Manuscript ID	JACERS-48241
Manuscript Type:	Research Article
Date Submitted by the Author:	24-Aug-2021
Complete List of Authors:	Wang, Yuanyuan; Shanghai University of Engineering Science LIU, Hongbo; Shanghai University of Engineering Science Yan, Tingnan; Shenzhen Institutes of Advanced Technology Chinese Academy of Sciences Zhao, Jianwei; Shenzhen Institutes of Advanced Technology Chinese Academy of Sciences Guo, Shifeng; Shenzhen Institutes of Advanced Technology Chinese Academy of Sciences Lu, Zhilun; The University of Sheffield, materials science and engineering Wang, Dawei; University of Sheffield, Department of Materials Science and Engineering;
Keywords:	dielectric materials/properties, activation energy, core-shell structures
Author-supplied Keyword: If there is one additional keyword you would like to include that was not on the list, please add it below::	SrTiO3

Microstructure and electrical properties of Nb-doped $SrTiO_3$-based lead-free ceramics

Yuanyuan Wang[a,b], Hongbo Liu[a]*, Tingnan Yan[b], Jianwei Zhao[b], Shifeng Guo[c], Zhilun Lu[d,e]*, Dawei Wang[b]*

[a]*School of Materials Engineering, Shanghai University of Engineering Science, Shanghai 201620, China*

[b]*Shenzhen Institute of Advanced Electronic Materials, Shenzhen Institute of Advanced Technology, Chinese Academy of Sciences, Shenzhen 518055, China*

[c]*Shenzhen Key Laboratory of Smart Sensing and Intelligent Systems, Shenzhen Institute of Advanced Technology, Chinese Academy of Sciences, Shenzhen, 518055, China*

[d]*Department of Materials Science and Engineering, University of Sheffield, Sheffield, S1 3JD, UK*

[e]*The Henry Royce Institute, Sir Robert Hadfield Building, Sheffield, S1 3JD, UK*

* Author to whom correspondence should be addressed:

bohongliu@gmail.com; zhilun.lu@sheffield.ac.uk; wangdawei102@gmail.com

Abstract:

In this work, Nb-doped $0.75SrTiO_3$-$0.25BiFeO_3$ (ST-BF) lead-free ceramics are designed and synthesized using a conventional solid state sintering method. The influence of Nb doping on the microstructure, dielectric and electrical properties are systematically investigated. As increasing the Nb concentration, the crystal structure of ST-BF remains cubic phase as exhibited in XRD patterns. The average grain size is found to increase from 0.33 μm to 6.23 μm, and then decrease to 1.88 μm by Nb doping, along with clear core-shell microstructure. A relatively low dielectric loss (~0.1, at 1 kHz) and a stable dielectric constant (~700, at 1 kHz) are obtained for the 0.03Nb-doped ST-BF composition at room temperature. Further impedance analysis shows that the doping of Nb increases the total impedance, forming an electrically conductive core and a non-conductive shell, with an enhanced activation energy. The results may provide a feasible approach to develop novel ST-based lead-free dielectric ceramics for capacitor applications.

Keywords: $SrTiO_3$, $BiFeO_3$, core-shell microstructure, impedance, dielectric properties

Introduction

Dielectric ceramics are widely used to manufacture various electronic devices, such as capacitors, thermistors, actuators, etc., and there is an urgent need to develop novel dielectric ceramics with excellent performance.[1, 2] $BiFeO_3$ (BF) is a room temperature multiferroic material with a high Curie temperature and large polarization. However, the single-phase BF can only exist stably in a limited and narrow temperature range.[3, 4, 5] Paraelectric $SrTiO_3$ (ST) belongs to linear dielectrics and possesses unique physical properties, such as a moderate dielectric constant (ε′), a relatively high breakdown strength (BDS) and a low dielectric loss (tanδ).[6, 7, 8, 9] Both ST and BF belong to the same crystal structure with the molecular formula of ABO_3, and their combination shows potential versatility and applications. For example, Ren *et al.* reported that Mn substituting Fe site could effectively reduce tanδ, improving the BDS and magnetization of 0.5BF-0.5ST ceramics.[5] Lu *et al.* presented that 0.4ST-0.6BF-0.01Nb solid solution showed high ε′ (~2500) at ~380°C, maximum polarization (P_{max}) ~52.7 μC cm^{-2} and electrostrain (S_{max}) ~0.15%.[10] Lu *et al.* also showed that the high conductivity of BF-ST could be effectively suppressed by Nb doing, and 0.03Nb-doped 0.5BF-0.4ST-$0.1BiMg_{2/3}Nb_{1/3}O_3$ ceramics possessed a large recoverable energy density of 8.2 J cm^{-3} at an electric field of 460 kV cm^{-1}.[11]

However, most researches on ST-BF ceramics focus on the BF-rich compositions, and there is a lack of reports on the ST-rich compositions.[12, 13] In this work, ST-BF ceramics with a composition of 0.75ST-0.25BF-xNb (x =0.00, 0.01, 0.02, 0.03, 0.04, 0.05 and 0.06) were prepared and investigated. The effects of Nb content on the phase structure, microstructure, dielectric, and electrical properties of ST-BF lead-free ceramics are thoroughly studied.

Experimental

0.75ST-0.25BF-xNb (x =0.00, 0.01, 0.02, 0.03, 0.04, 0.05 and 0.06) ceramics were prepared by the conventional solid state reaction method. Analytical-grade raw chemicals Bi_2O_3 (Macklin, AR), Fe_2O_3 (Aladdin, ≥99%), $SrCO_3$ (Aladdin, 99.5%), TiO_2 (Macklin, 99%) and Nb_2O_5 (Aladdin, 99.9%) were weighted stoichiometrically, and ball-milled for 24 h with ethanol as solvent and zirconia balls as medium. After drying, the mixed powder was calcined at 850℃ for 3 h in air atmosphere, followed by a secondary ball-milling for 12 h. With the usage of a binder (Polyvinyl Alcohol solution), the calcined powder was pressed into pellets (10 mm in diameter) under a hydraulic pressure of 200 MPa. The pellets were then sintered at 1250-1300℃ for 3 h, buried with sacrificing powder with the same composition to reduce the volatilization of Bi.

The density of the sintered ceramics was measured using the Archimedes method. The crystal structure of the samples was characterized by X-ray diffraction (XRD, Rigaku Smart Lab, Japan) in a 20-80° 2θ range. The lattice parameters of ST-BF-xNb ceramics were obtained through Rietveld refinement by a software of GSAS-II.[14] Scanning electron microscopy (Apreo 2 SEM, Thermo Fisher Scientific, Waltham, MA) was performed to probe microstructure of the sintered pellets. The average grain size was statistically calculated upon different compositions. Electrical and dielectric properties were measured by a precision impedance analyzer (Agilent E4980A, Santa Clara, CA) with a frequency range of 100 Hz-2 MHz and a temperature range of 25-500℃, using pellets with coated silver electrodes on opposing parallel surfaces.

Results and discussion

The XRD patterns of ST-BF-xNb (x=0.00≤x≤0.06) ceramics are shown in Figure 1(a). All specimens possess a perovskite cubic structure without the trace of an impurity phase. With the increase of Nb concentration, there is no splitting of (100) and (200) peaks, whereas a slight shifting of diffraction peaks to the lower angle is observed, which is mainly attributed to the expansion of lattice volume. Theoretically, the lattice expansion is induced by the replacement of Ti^{4+} (0.605 Å) and Fe^{3+} (0.55 Å) by a larger ionic radius of Nb^{5+} (0.64 Å) in the 6-fold coordination.[8, 15] To further clarify the crystal structure, Rietveld refinement is performed based on the $Pm\bar{3}m$ space group, as given in Figure 1(b) and (c), and the refined lattice parameters are listed in Table I. The value of R_{wp} is less than 15%, implying that the refined data is matched well with the raw XRD data. The lattice parameters and unit cell volume are found to increase with increasing Nb content, which tend to be stable above x=0.03.

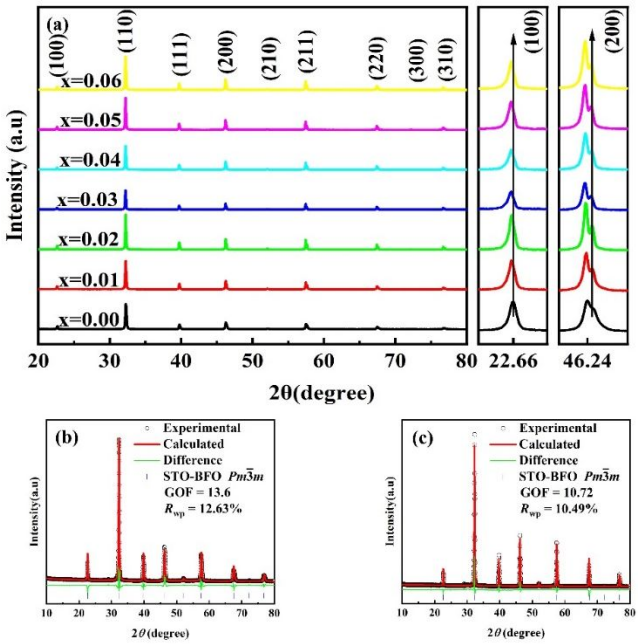

Figure 1. (a) XRD patterns of ST-BF-xNb ($0.00 \leq x \leq 0.06$) ceramics at room temperature. Rietveld refinement results of the observed XRD patterns for (b) x=0.00 and (c) x=0.03.

Table I. Rietveld refinement results for ST-BF-xNb ceramics.

x	GOF	R_{wp}(%)	Space group	*a* (Å)	Cell volume (Å^3)
0.00	13.2	12.63	$Pm\bar{3}m$	3.91958	60.217
0.01	7.89	8.07	$Pm\bar{3}m$	3.92377	60.322
0.02	14.81	14.34	$Pm\bar{3}m$	3.92437	60.438
0.03	10.72	10.49	$Pm\bar{3}m$	3.92532	60.482
0.04	15.28	14.96	$Pm\bar{3}m$	3.92512	60.473
0.05	12.25	11.7	$Pm\bar{3}m$	3.92519	60.476
0.06	10.04	9.64	$Pm\bar{3}m$	3.92531	60.481

Figure 2 presents the SEM images of the surfaces for ST-BF-xNb ceramics with different Nb contents. All samples exhibit a dense morphology with a small portion of pores. According to the refined lattice parameters and measured bulk densities of the ceramics, the calculated relative densities of the sintered ceramics are all higher than 90%, which are in agreement with the SEM results. Furthermore, with the increase of Nb content, the average grain size increases from 0.33 um to 6.23 um and then decreases after exceeding 3%Nb, suggesting that a small amount of Nb doping promotes the grain growth but then suppresses it after reaching the limitation of solid solution.

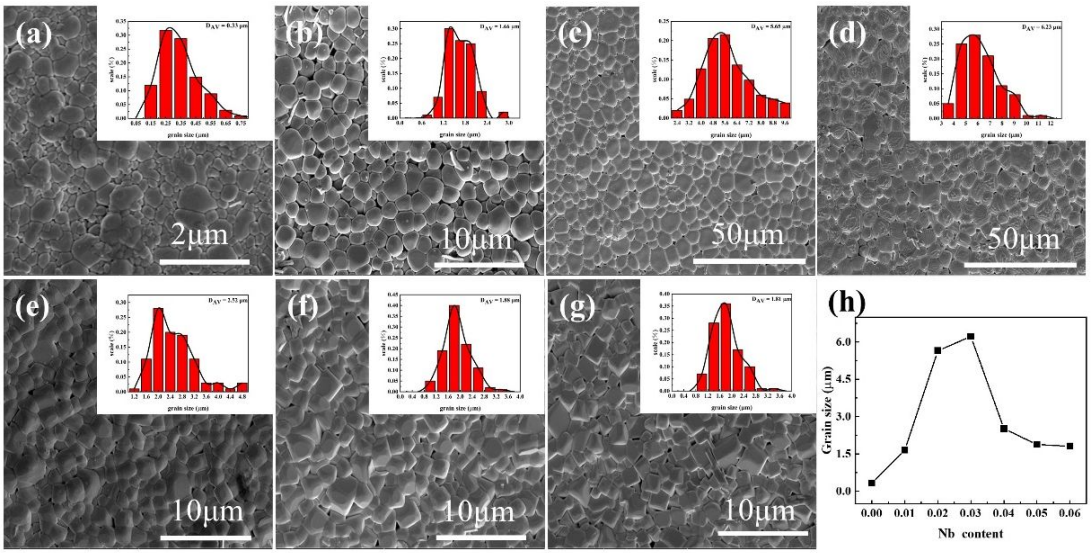

Figure 2. The surface morphology and grain size distribution of ST-BF-xNb ceramics with x = (a) 0.00, (b) 0.01, (c) 0.02, (d) 0.03, (e) 0.04, (f) 0.05 and (g) 0.06. (h) Average grain size as a function of x content.

Backscattered electron (BSE) images of the polished surfaces for ST-BF-xNb ceramics are shown in Figure 3. It is clear that all ceramics exhibit a heterogeneous microstructure (bright and dark contrast), with chemically obvious core-shell microstructure in grains and a small amount of secondary phase existing at grain boundaries, which are commonly observed in BF-based ceramics as reported previously.[16, 17, 18, 19] To further probe the chemical heterogeneity, energy dispersive spectroscopy (EDS) is performed on the finely polished surfaces and the results for ST-BF-0.03Nb ceramic are displayed in Figure 4. The results show that Bi and Fe are rich in cores and grain boundaries, which is consistent to the bright and dark contrast in the BSE images (Figure 3).

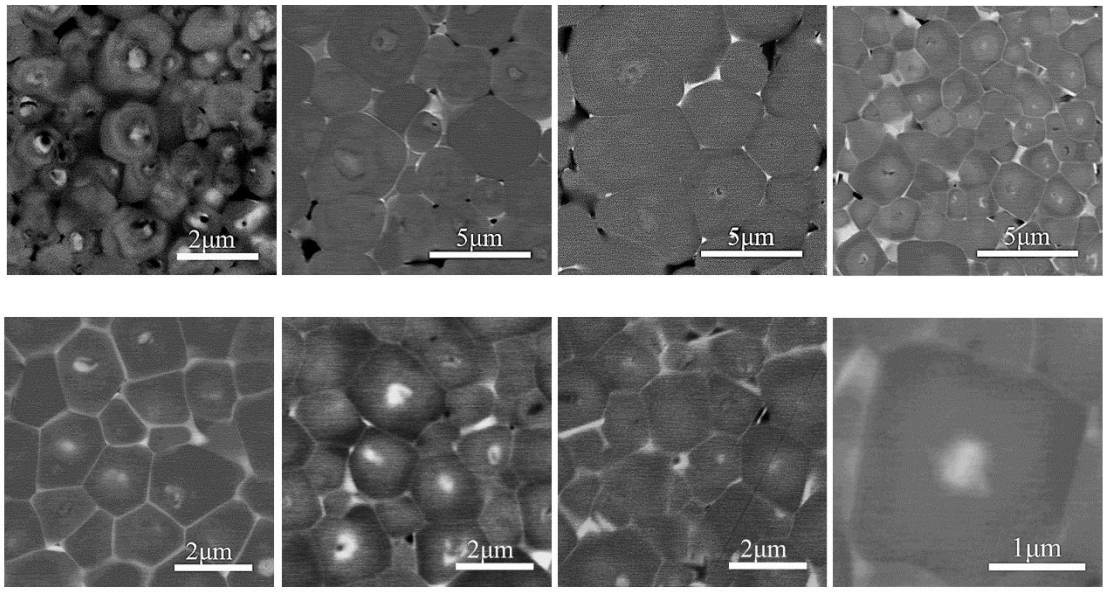

Figure 3. BSE images of polished surfaces for ST-BF-xNb ceramics with x = (a) 0.00, (b) 0.01, (c) 0.02, (d) 0.03, (e) 0.04, (f) 0.05 and (g) 0.06; (h) Enlarged image for x = 0.03.

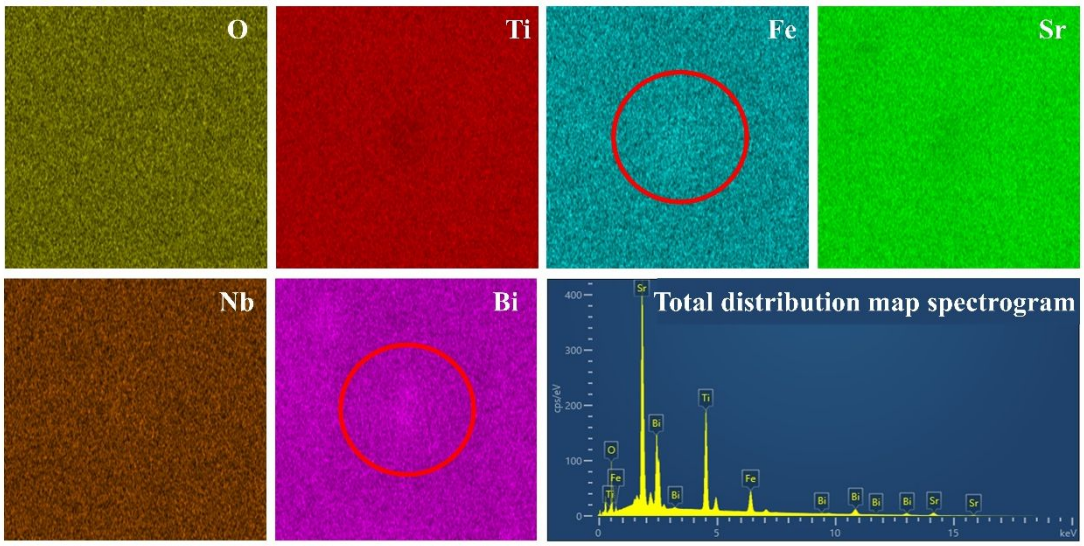

Figure 4. Elemental mappings for ST-BF-0.03Nb ceramics.

Figure. 5 shows the frequency dependence of dielectric properties (ε′ and tanδ) for ST-BF-xNb ceramics in the frequency range of 100 Hz-1 MHz at room temperature. At low frequencies, the values of ε′ and tanδ are high, mainly originated from the space charge polarization. ε′

decreases rapidly with increasing the frequency and almost remains a constant at higher frequencies, which is mainly attributed to the slow movement of induced dipoles under the application of an electric field, along with decreased tanδ with increasing frequency.[20] The values of ε′ and tanδ as a function of Nb content at 1 kHz are plotted in Figure 5(c,d). The decrease in ε′ and tanδ evidences that Nb doping significantly reduces the leakage current of ST-BF ceramics, which is benefited from the intrinsic dipole polarization.

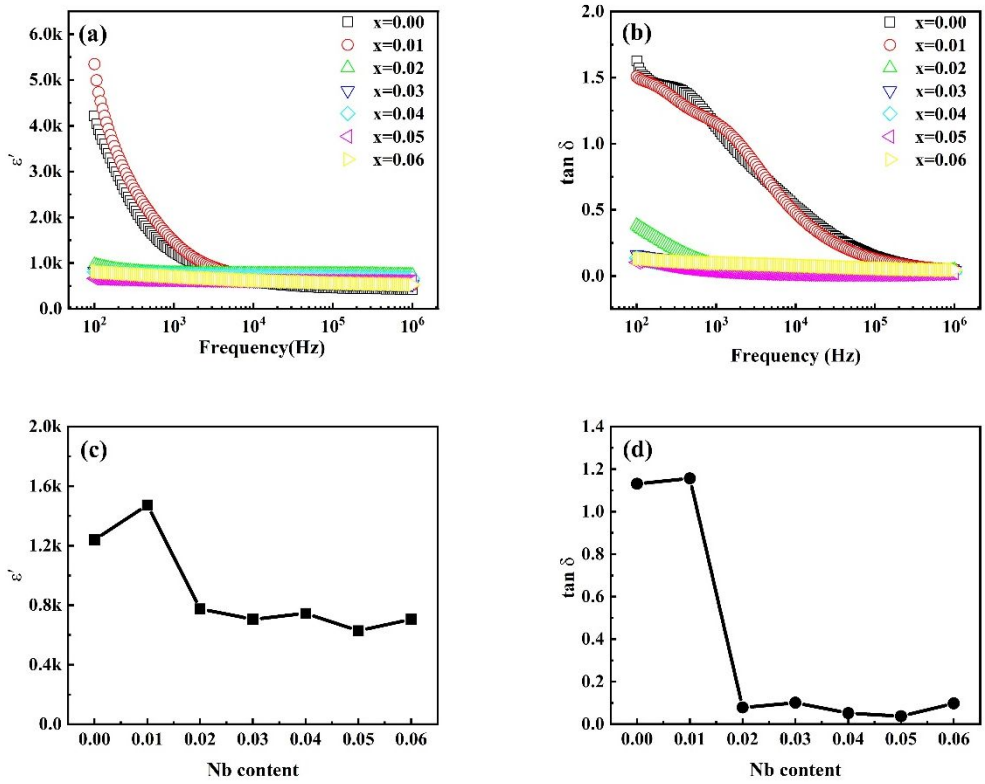

Figure 5. Frequency dependence of (a) ε′ and (b) tanδ for ST-BF-xNb ceramics; (c) ε′ and (d) tanδ as a function of Nb content at 1 kHz.

Impedance spectroscopy is employed to study the electrical microstructure of ST-BF-xNb (0.00≤x≤0.06) ceramics. Impedance complex plane (Z*) plots for ST-BF-xNb (0.02≤x≤0.06, insert graph x=0.00 and 0.01 at 50℃) ceramics at 300℃, are plotted in Figure 6. Non-typical

semicircles appear at near room temperature for x=0.00 and 0.01, which displays that 1 mol% Nb doping is not sufficient to suppress the leakage current. However, for x≥0.02 the semicircles can only be observed at high temperature (e.g. 300℃), and with the increase of Nb doping amount, the diameter of semicircle increases and reaches a maximum at x=0.03 and then decreases gradually, which reveals that the lowest electrical conductivity and optimized doping concentration is 3 mol%, and higher doping level (x>0.03) doesn't reduce the total electrical conductivity further. In addition, these non-typical semicircles should consist of at least two semicircles signifying different electroactive components, indicating electrical heterogeneity of the ceramics.[11]

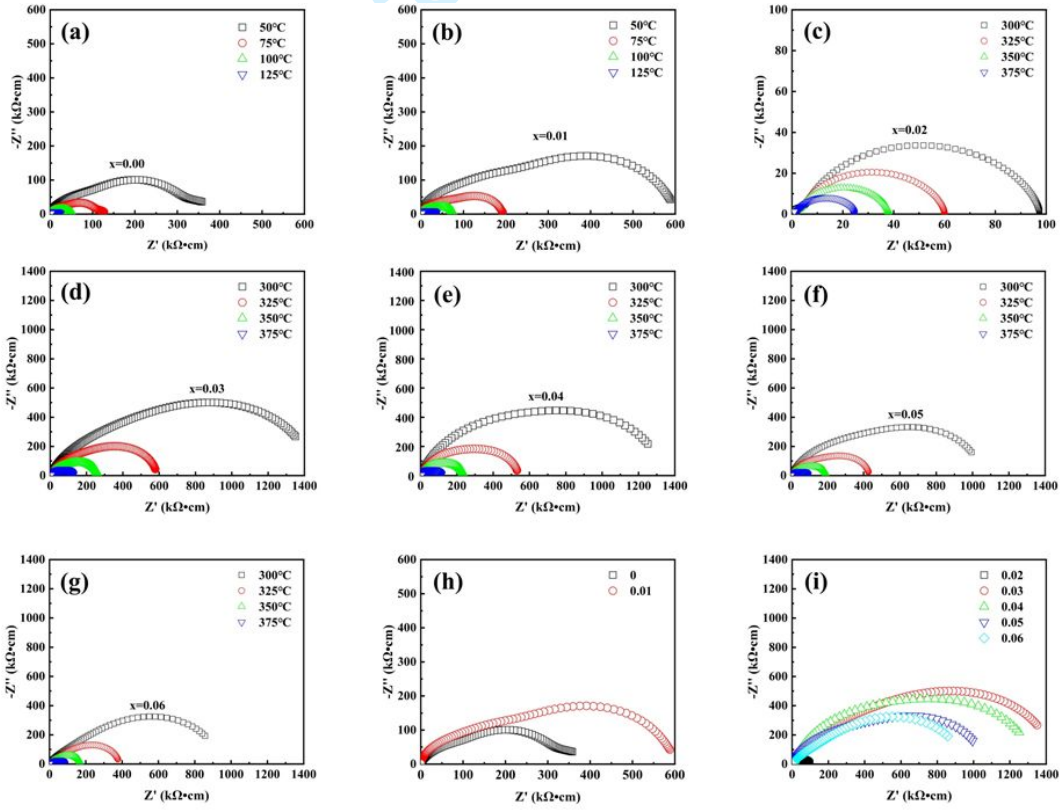

Figure 6. Temperature-dependent Z* plots for ST-BF-xNb ceramics with x = (a) 0.00, (b) 0.01, (c) 0.02, (d) 0.03, (e) 0.04, (f) 0.05 and (g) 0.06; (h)Z* plots for ST-BF-xNb (x=0.00-0.06) ceramics at 300℃ (insert: x=0.00 and 0.01 at 50 ℃).

Therefore, the combined spectra of Z" and M" are used to further investigate the electrical heterogeneity, as given in Figure 7. To locate more electrical components at the same temperature, 50℃ and 300℃ data is selected for x=0.00-0.01 and x=0.02-0.06, respectively. As shown in Figure 7, two main peaks and one small peak (two in Z" and one in M" for x=0.00-0.01 at 50℃ and one in Z" and two in M" for x=0.02-0.06 at 300℃) can be observed for all samples, which suggest that there are three electroactive components those can be treated as three parallel resistor-capacitor elements connected in series.[21] These three observed components in all ceramics are also consistent with the non-typical semicircles in Z* plots (Figure 6), revealing Nb doping does not significantly improve the electrical homogeneity. The extracted resistivity (R) and capacitivity (C) of these three components are list in Table Ⅱ. The capacitivities extracted from low to high frequency peaks are 0.8-3.0 nF cm^{-1}, 100-400 pF cm^{-1} and 50-80 pF cm^{-1}, which correspond to grain boundary, shell and core, respectively[22] and agree well with the observation of core-shell microstructure in grains presented in Figure 3. Compared Figure 6(h) with Figure 6(i), the M" peak appears at higher temperature for x=0.03, which means that appropriate Nb doping (3 mol%) can reduce the electrical conductivity of core for ST-BF. And combined Figure 7 and Table Ⅱ, it should be noted that x≥0.02 Nb doping significantly decreases the electrical conductivity of grain boundary, slightly reduces the conductivity of shell, but has little effect on the conductivity of core with increasing the Nb concentration.

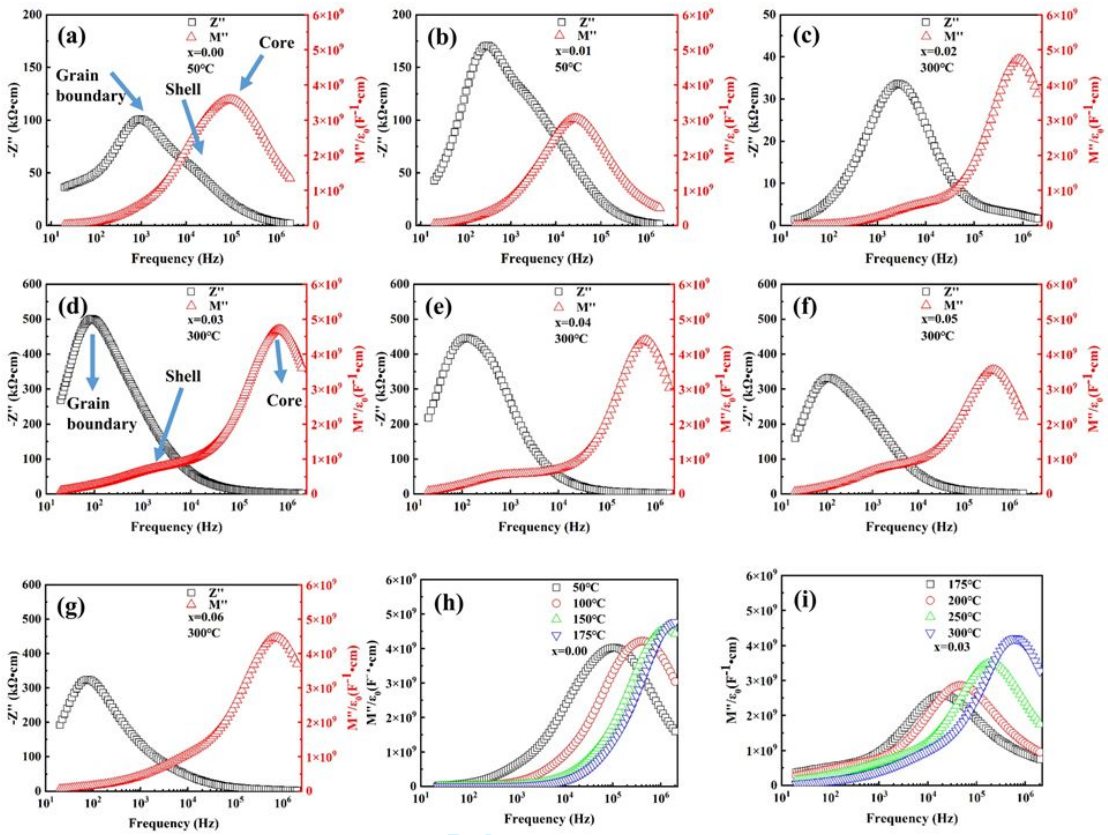

Figure. 7. Combined Z" and M" spectroscopic plots at 50℃ for x = (a) 0.00, (b) 0.01, at 300℃ for x = (c) 0.02, (d) 0.03, (e) 0.04, (f) 0.05 and (g) 0.06; Temperature-dependent M" spectroscopic plots for x = (h) 0.00 and (i) 0.03.

Table Ⅱ. The values of R and C for each component at 75 and 300℃ derived based on the Z" and M" peak values.

Composition	Component 1 (Grain Boundary)		Component 2 (Shell)		Component 3 (Core)	
	R (kΩ·cm)	C (F cm^{-1})	R (kΩ·cm)	C (F cm^{-1})	R (kΩ·cm)	C (F cm^{-1})
0 (50℃)	202	8.50×10^-10	114	1.16×10^-10	23.4	6.98×10^-11
0.01 (50℃)	342	1.6×10^-9	246	2.75×10^-10	71.8	8.19×10^-11
0.02 (300℃)	67.3	8.95^-10	46.7	4.03×10^-10	3.81	5.29×10^-11
0.03 (300℃)	1000	1.87^-9	118	2.94×10^-10	4.24	5.32×10^-11
0.04 (300℃)	892	1.39^-9	380	4.51×10^-10	4.48	5.68×10^-11
0.05 (300℃)	664	2.10^-9	234	3.25×10^-10	5.12	7.05×10^-11

0.06 (300℃)	649	3.04^-9	55.5	2.13×10^-10	4.05	5.59×10^-11

The Arrhenius plots and activation energies of ST-BF-xNb ($0.0 \leq x \leq 0.06$) ceramics are given in Figure 8 and Table Ⅲ. We can separate the compositions to three groups based on their electrical properties. The first group is x=0.00-0.01, which indicates that 1 mol% Nb doping decreases the conductivity slightly but not helpful for the increase of activation energies. The second group is x=0.02. When Nb doping concentration reaches 2 mol%, the conductivity of grain boundary, shell and core all decreases significantly with enhanced activation energies. The last group is x=0.03-0.06. As increasing the Nb amount to 3 mol%, the conductivity energy of grain boundary, shell and core reach minimum with the optimized activation energy. At x>0.03, the Nb doping doesn't effectively reduce the electrical conductivity and enhance the activation energy of ST-BF-xNb ceramics.

Table Ⅲ. The activation energies of ST-BF-xNb ($0.0 \leq x \leq 0.06$) ceramics.

Component	**Grain Boundary**	**Core**	**Shell**
x=0.00	0.42eV	0.36eV	0.28eV
x=0.01	0.43ev	0.40eV	0.35ev
x=0.02	0.59eV	0.61eV	0.35eV
x=0.03	1.06eV	0.87eV	0.47eV
x=0.04	1.04eV	0.89eV	0.48eV
x=0.05	1.04eV	0.72eV	0.52eV
x=0.06	1.06eV	0.49eV	0.44eV

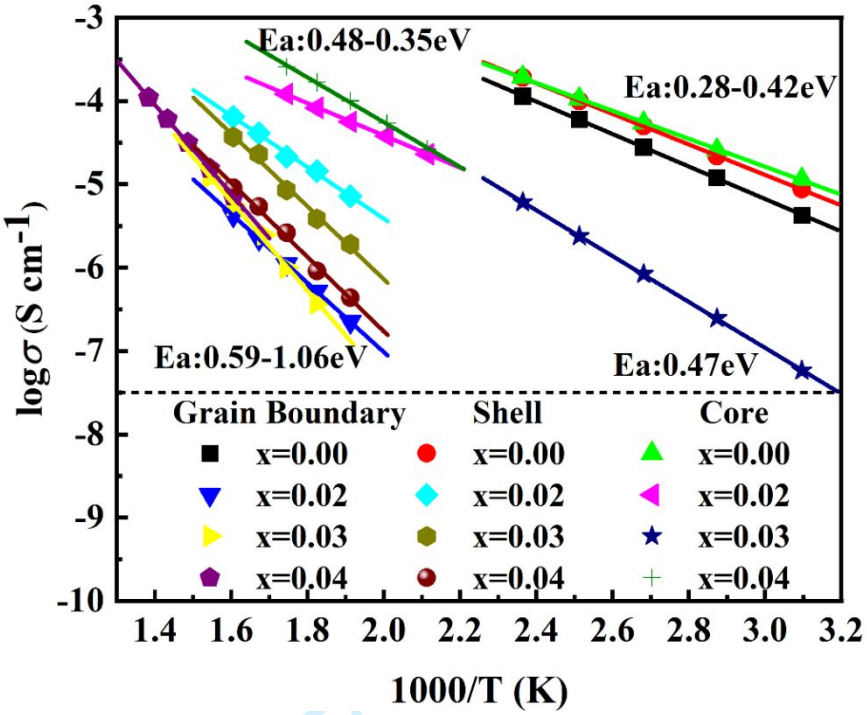

Figure 8. Arrhenius plots of ST-BF-xNb (0.0≤x≤0.06) ceramics.

Conclusions

In this work, ST-BF-xNb (x=0.00~0.06) lead-free ceramics are studied from the aspects of crystal structure, microstructure and functional properties. From the XRD patterns, the addition of Nb does not change the cubic phase but cause the distortion of crystal lattice. BSE and EDS results evidence that a core-shell microstructure is formed (heterogeneity inside grains), and a Bi-rich secondary phase is formed at grain boundaries. The impedance results indicate that dielectric constant and loss increases initially and then decreases to a stable state with the increase of Nb content. When x=0.03, the total resistivity of the sample is the largest, and the dielectric properties are also optimized. Furthermore, it is found that the doping of Nb effectively suppresses the total conductivity of the core-shell structure for ST-BF ceramics,

forming a relatively conductive cores and non-conductive shells, which play an important role in the change of electrical properties.

Acknowledgements

The work is supported by the National Natural Science Foundation of China (Grant No. 11704242) and Natural Science Foundation of Shanghai, China (Grant No. 17ZR1447200).

References

1. Y. Lin, D. Li, M. Zhang, and H. Yang, "(Na0.5Bi0.5)0.7Sr0.3TiO3 modified by Bi(Mg2/3Nb1/3)O3 ceramics with high energy-storage properties and an ultrafast discharge rate," *Journal of Materials Chemistry C,* 8[7] 2258-64 (2020).
2. F. Kang, L. Zhang, B. Huang, P. Mao, Z. Wang, Q. Sun, J. Wang, and D. Hu, "Enhanced electromechanical properties of SrTiO3-BiFeO3-BaTiO3 ceramics via relaxor behavior and phase boundary design," *Journal of the European Ceramic Society,* 40[4] 1198-204 (2020).
3. D. Wang, M. Wang, F. Liu, Y. Cui, Q. Zhao, H. Sun, H. Jin, and M. Cao, "Sol–gel synthesis of Nd-doped BiFeO3 multiferroic and its characterization," *Ceramics International,* 41[7] 8768-72 (2015).
4. Z.-J. Li, Z.-L. Hou, W.-L. Song, X.-D. Liu, D.-W. Wang, J. Tang, and X.-H. Shao, "Mg-substitution for promoting magnetic and ferroelectric properties of BiFeO 3 multiferroic nanoparticles," *Materials Letters,* 175 207-11 (2016).
5. Y. Ren, H. Liu, F. Liu, and G. Liu, "Tuning of electric and magnetic properties of BiFeO3-SrTiO3 solid solution ceramics by site-specific doping of Mn," *Journal of Alloys and Compounds,* 877 (2021).
6. H. Yang, F. Yan, Y. Lin, and T. Wang, "Novel Strontium Titanate-Based Lead-Free Ceramics for High-Energy Storage Applications," *ACS Sustainable Chemistry & Engineering,* 5[11] 10215-22 (2017).
7. Q.-G. Hu, Z.-Y. Shen, Y.-M. Li, Z.-M. Wang, W.-Q. Luo, and Z.-X. Xie, "Enhanced energy storage properties of dysprosium doped strontium titanate ceramics," *Ceramics International,* 40[1] 2529-34 (2014).
8. F. Yan, H. Yang, Y. Lin, and T. Wang, "Dielectric and Ferroelectric Properties of SrTiO3-Bi0.5Na0.5TiO3-BaAl0.5Nb0.5O3 Lead-Free Ceramics for High-Energy-Storage Applications," *Inorg Chem,* 56[21] 13510-16 (2017).
9. M. Qin, F. Gao, J. Cizek, S. Yang, X. Fan, L. Zhao, J. Xu, G. Dong, M. Reece, and H. Yan, "Point defect structure of La-doped SrTiO3 ceramics with colossal permittivity," *Acta Materialia,* 164 76-89 (2019).

10. Z. Lu, G. Wang, L. Li, Y. Huang, A. Feteira, W. Bao, A. K. Kleppe, F. Xu, D. Wang, and I. M. J. M. T. P. Reaney, "In situ poling X-ray diffraction studies of lead-free BiFeO3–SrTiO3 ceramics," 19 100426 (2021).
11. Z. Lu, G. Wang, W. Bao, J. Li, L. Li, A. Mostaed, H. Yang, H. Ji, D. Li, A. Feteira, F. Xu, D. C. Sinclair, D. Wang, S.-Y. Liu, and I. M. Reaney, "Superior energy density through tailored dopant strategies in multilayer ceramic capacitors," *Energy & Environmental Science,* 13[9] 2938-48 (2020).
12. L. Li, H. Liu, G. Wen, and G. Liu, "Structural evolution and dielectric response of (1-x)BiFeO3-xSrTiO3 ceramics," *Ceramics International,* 44 S69-S71 (2018).
13. H. Liu and X. Yang, "Structural, dielectric, and magnetic properties of BiFeO3-SrTiO3 solid solution ceramics," *Ferroelectrics,* 500[1] 310-17 (2016).
14. B. H. Toby and R. J. J. o. A. C. Dr Ee Le, "GSAS-II: the genesis of a modern open-source all purpose crystallography software package," 46[2] 544-49 (2013).
15. B. Zhong, Z. Long, C. Yang, Y. Li, and X. Wei, "Colossal dielectric permittivity in co-doping SrTiO3 ceramics by Nb and Mg," *Ceramics International,* 46[12] 20565-69 (2020).
16. G. Wang, J. Li, X. Zhang, Z. Fan, F. Yang, A. Feteira, D. Zhou, D. C. Sinclair, T. Ma, X. Tan, D. Wang, and I. M. Reaney, "Ultrahigh energy storage density lead-free multilayers by controlled electrical homogeneity," *Energy & Environmental Science,* 12[2] 582-88 (2019).
17. D. Wang, Z. Fan, W. Li, D. Zhou, A. Feteira, G. Wang, S. Murakami, S. Sun, Q. Zhao, X. Tan, and I. M. Reaney, "High Energy Storage Density and Large Strain in Bi(Zn2/3Nb1/3)O3-Doped BiFeO3–BaTiO3 Ceramics," *ACS Applied Energy Materials,* 1[8] 4403-12 (2018).
18. G. Wang, Z. Lu, H. Yang, H. Ji, A. Mostaed, L. Li, Y. Wei, A. Feteira, S. Sun, D. C. Sinclair, D. Wang, and I. M. Reaney, "Fatigue resistant lead-free multilayer ceramic capacitors with ultrahigh energy density," *Journal of Materials Chemistry A,* 8[22] 11414-23 (2020).
19. D. Wang, G. Wang, S. Murakami, Z. Fan, A. Feteira, D. Zhou, S. Sun, Q. Zhao, and I. M. Reaney, "BiFeO3-BaTiO3: A new generation of lead-free electroceramics," *Journal of Advanced Dielectrics,* 08[06] (2019).
20. N. H. Patel, M. Shah, D. D. Shah, and P. K. Mehta, "Effect of doping in SrTiO3:BiFeO3 binary system," *Materials Today: Proceedings* (2020).
21. H. Yang, Z. Lu, L. Li, W. Bao, H. Ji, J. Li, A. Feteira, F. Xu, Y. Zhang, H. Sun, Z. Huang, W. Lou, K. Song, S. Sun, G. Wang, D. Wang, and I. M. Reaney, "Novel BaTiO3-Based, Ag/Pd-Compatible Lead-Free Relaxors with Superior Energy Storage Performance," *ACS Appl Mater Interfaces,* 12[39] 43942-49 (2020).
22. D. J. T. S. Irvine, D. D. C. Sinclair, and P. A. R. West, "Electroceramics: Characterization by Impedance Spectroscopy " *Advanced Materials,* 2[3] 132-38 (1990).